Six-dimensional model of icosahedral Al-Pd-Mn quasicrystals

Akiji Yamamoto and Hiroyuki Takakura
Advanced Materials Laboratory, National Institute for Materials Science, Tsukuba, Ibaraki, 305, Japan

An Pang Tsai
Materials Engineering Laboratory, National Institute for Materials Science, Tsukuba, Ibaraki, 305, Japan
(Received 30 October 2002; revised manuscript received 19 May 2003; published 4 September 2003)

A six-dimensional cluster model of icosahedral Al-Pd-Mn (i-Al-Pd-Mn) quasicrystals used in the recent structure refinement is described in detail. This model is based on five kinds of clusters located at vertices, edge centers of the inflated three-dimensional Penrose pattern (3DPP) with an edge length of about 20 Å, and two body-diagonal positions of each acute rhombohedron. Two kinds of 20 Å clusters, one of which is seen in β-Al-Pd-Mn-Si, are located at even- and odd-parity 12-fold vertices of the inflated 3DPP. This is proved to give small R factors ($R_w=0.055$, $R=0.049$) for 493 independent reflections and leads to the 1/1 and 2/1 approximant structures of i-Al-Pd-Mn (α- and β-Al-Pd-Mn-Si) by introducing appropriate cubic phason strains and taking a three-dimensional cut.

DOI: 10.1103/PhysRevB.68.094201 PACS number(s): 61.44.Br, 36.40.Mr, 61.66.Dk

I. INTRODUCTION

Since the report of the discovery[1] of icosahedral Al-Mn (i-Al-Mn) quasicrystals in 1984, extensive studies have been made toward the structure determinations of quasicrystals.(See Refs. 2 and 3 and references therein.) In particular, the single-domain quasicrystals first found in i-Al-Cu-Fe (Ref. 4) made it possible to determine their detailed structures in principle. However, theoretical difficulties still remain because there are no established methods of description or parametrizations of the quasicrystals. It is clear that in order to describe aperiodic crystal structures such as quasicrystals, the description in a higher-dimensional space is inevitable. Then a nonperiodic structure in the three-dimensional (3D) space can be given as a 3D intersection of a higher-dimensional periodic structure.[5–7] As a result, the number of parameters necessary for the structure description becomes finite. Early works of the structure determination were based on simple large occupation domains (OD's, windows, atomic surfaces) placed at high symmetric points (Wyckoff positions, special positions) in a higher-dimensional space.[8–11] Such a model can explain the intensity of strong reflections, but a large data set given by the single-crystal method clarified that it is not sufficient to describe detailed quasicrystal structures. In order to describe the structure more accurately, it is very important to introduce the atom shift from the ideal position that is assumed in early works because diffraction experiments are very sensitive to the position of atoms. In order to introduce the shift parameters, one of the authors (A.Y.) proposed a higher-dimensional cluster model at an early stage.[12] This was recently proved to be efficient for describing detailed structures of quasicrystals by the successful structure refinements for decagonal Al-Mn-Pd (d-Al-Mn-Pd), d-Al-Ni-Co, and i-Al-Pd-Mn.[13–15]

The icosahedral quasicrystals have several structures with different space groups. They are roughly classified by the lattice constant a and their space group. The first-found icosahedral Al-Mn (i-Al-Mn) has $a \simeq 4.6$ Å and space group $Pm\overline{3}\overline{5}$.[8] i-Al-Cu-Li also belongs to this type.[16,17] Another type has a doubled lattice constant a and the space group $Fm\overline{3}\overline{5}$. The third type has a 2τ-times larger a than that of the first type with space group[18] $Pm\overline{3}\overline{5}$ [$\tau=(1+\sqrt{5})/2$]. Their detailed structures are not yet known except for i-Al-Pd-Mn, solved recently. This belongs to the second type and this is the key structure for understanding icosahedral quasicrystals. Most icosahedral quasicrystals of good quality belong to this type and the third type can be considered as its superstructure. On the other hand, the quality of quasicrystals in the first type is generally poor except for Cd-based icosahedral quasicrystals and i-Zn-Mg-Sc found recently.[19,20] Therefore we analyzed the i-Al-Pd-Mn structure in the second type first in the series of icosahedral quasicrystal analyses in progress.

A few structure determinations of icosahedral quasicrystals including i-Al-Pd-Mn have been tried by powder diffraction and single-crystal methods.[10,11,21–23] In these analyses, large OD's with spherical/ellipsoidal or polyhedral shape were used. Atom positions were fixed at some ideal positions and their occupation probabilities and thermal parameters were refined. In the case of spherical OD's, the size of OD's was also refined. This treatment sometimes causes very short interatomic distances because of the violation of the closeness conditions.[21] If we assume OD's with simple polyhedral shape, many kinds of incomplete clusters arise,[24] which are a part of the cluster with the highest symmetry. It seems that all quasicrystals consist of a few kinds of clusters with high symmetry at least to a good approximation. This is in particular evident in decagonal quasicrystals. In this case, each cluster has a fivefold or tenfold symmetry.[25–27] Therefore it is important to obtain a model consisting of several clusters with icosahedral symmetry for icosahedral quasicrystals. We proposed such a model in a higher-dimensional space (higher-dimensional cluster model) for i-Al-Pd-Mn (Refs. 28 and 29) and refined the structure based on x-ray data.[15,30]

In contrast to other models, the higher-dimensional cluster model has very complicated OD's that consist of several small OD's related to the OD's for the cluster centers. Each

small OD generates atom positions with the same local environment. Therefore, we can assume the same occupation probability and thermal parameter for all such atoms. If the small OD is not on the special position with very high site symmetry, the shift of the OD along some external (physical or parallel) space directions is allowed. This enables us to give the refinement of the atom coordinates in a cluster. Recent analyses based on such a cluster model gave successful results for decagonal Al-Ni-Co (d-Al-Ni-Co) and i-Al-Pd-Mn quasicrystals, indicating the importance of the refinement of atom positions. The R_w and R factors of 0.045 and 0.063 for 449 independent reflections are obtained for d-Al-Co-Ni (103 parameters), showing that the structure is reliable. For i-Al-Pd-Mn, a cluster model gave the R_w and R factors of 0.055 and 0.049 for 493 independent reflections (about 100 parameters). The latter is the first successful structure refinement for icosahedral quasicrystals, which is relatively difficult compared with the refinement of decagonal quasicrystals.

In the icosahedral quasicrystals, there exist the cubic 1/1 and 2/1 approximants in some cases, which have the lattice constants of about 12 and 20 Å. It is well known that the α phase of Al-Mn (α-Al-Mn) and R-Al-Cu-Li are the examples of the 1/1 approximants in i-Al-Mn and i-Al-Cu-Li.[31] For considering quasicrystal structures based on approximant structures, the 2/1 approximant is more suitable than the 1/1 approximant, since the quasicrystal can be regarded as the crystal approximant with an infinite lattice constant. Although several 2/1 approximants have been found, most of them are only obtainable as powders. The only exceptional ones are the 2/1 approximants of i-Al-Pd-Mn and i-Al-Mg-Zn, single crystals of which have been grown recently. Their structures were determined based on x-ray single-crystal diffraction data.[32,33] In the latter, however, single-domain quasicrystal samples have not yet been obtained. The former shows that the approximant consists of an icosahedral cluster with a radius of about 20 Å. Our model of the i-Al-Pd-Mn is compatible with the 2/1 approximant: two kinds of large clusters are situated at the 12-fold vertices of the three-dimensional Penrose pattern (3DPP) with an edge length of about 20 Å. One of the clusters is quite similar to that in the 2/1 approximant.

In this paper we describe the six-dimensional (6D) cluster model used in the refinement of i-Al-Pd-Mn in detail and derive 1/1 and 2/1 approximant structures from the 6D model and compare with the real approximant structures. The detailed results of the structure refinement will be reported separately.

The paper is organized as follows. The 6D model building process based on diffraction experiments is shortly described in Sec. II. The guiding principle of the present model is explained in Sec. III. This model is built based on the 6D cluster model scheme in Sec. IV. The atom positions in the 3D space given by the model are shown in Sec. V. A general formulation for deriving crystal approximants by the linear phason is described shortly in Sec. VI and the 2/1 and 1/1 approximants are derived from the 6D model in Secs. VII and VIII. The model is compared with the model proposed by Katz and Gratias[24] in Sec. IX.

II. SIX-DIMENSIONAL MODEL BUILDING

It is well known that the icosahedral quasicrystals are described as a crystal (periodic structure) in 6D space.[6] We employ the coordinate system defined by the unit vectors $\mathbf{d}_i (i=1,2,\ldots,6)$ in the direct space,[7] which are given by

$$\mathbf{d}_1 = a_0 \mathbf{a}_3 + a_0' \mathbf{a}_6 ,$$

$$\mathbf{d}_i = a_0[(c_i \mathbf{a}_1 + s_i \mathbf{a}_2)s + c\mathbf{a}_3] + a_0'[(c_{2i}\mathbf{a}_4 + s_{2i}\mathbf{a}_5)s - c\mathbf{a}_6] \quad (i=2,3,\ldots,6), \tag{1}$$

where $c_i = \cos(2\pi i/5)$, $s_i = \sin(2\pi i/5)$, $c = \cos\theta = 1/\sqrt{5}$, $s = \sin\theta$, $\mathbf{a}_1, \mathbf{a}_2, \mathbf{a}_2$ and $\mathbf{a}_4, \mathbf{a}_5, \mathbf{a}_6$ are the unit vectors in the external (physical or parallel) and internal (complementary or perpendicular) spaces, respectively, and a_0 and a_0' are the lattice constants of the 6D icosahedral lattice. The lattice constant a_0 cannot be determined uniquely in quasicrystals because of the self-similarity of the icosahedral lattice[34,35] and a_0' is arbitrary.[7] We employ $a_0 = a_0' \simeq 4.8$ Å in this paper. Then, Eq. (1) can be written in the matrix form $\mathbf{d}_i = \sum_{j=1}^{6} Q_{ij}\mathbf{a}_\mathbf{j}$ with

$$Q = a_0 \begin{pmatrix} 0 & 0 & 1 & 0 & 0 & 1 \\ c_2 & s_2 & c & c_4 & s_4 & -c \\ c_3 & s_3 & c & c_1 & s_1 & -c \\ c_4 & s_4 & c & c_3 & s_3 & -c \\ 1 & 0 & c & 1 & 0 & -c \\ c_1 & s_1 & c & c_2 & s_2 & -c \end{pmatrix}. \tag{2}$$

We shortly describe the process of a 6D model building based on single-crystal x-ray data. First the location of large OD's can be estimated from the 6D Patterson map[36] or the recently developed low-density elimination method[37] (LDEM). In the present case, they are expected to be at (0,0,0,0,0,0), (1,0,0,0,0,0)/2, (1,1,1,1,1,1)/4, and/or (3,1,1,1,1,1)/4. Next, we can refine the size of each occupation domain assuming a spherical shape and an appropriate chemical arrangement for each domain. If necessary, a spherical OD is divided into several shells, each of which is occupied by a different atom.[11] This procedure can fix a rough size of each OD (or shell). In the present case, it was shown that there exist three large OD's at (0,0,0,0,0,0), (1,0,0,0,0,0)/2, and (3,1,1,1,1,1)/4 but no OD at (1,1,1,1,1,1)/4.[37] Finally, we can construct a cluster model based on the result of the refinement as discussed below. This makes the refinement of a cluster structure possible and can improve the R factor as shown in a separate paper. During the refinement, a small occupation domain was found at (1,0,0,0,0,0)/4.

III. HIGHER-DIMENSIONAL CLUSTER MODEL

The 6D model employed in the structure refinement of i-Al-Pd-Mn is a cluster model based on the 3DPP, where large clusters are located at the 12-fold vertices of the 3DPP with an edge length of about 20 Å. Its OD is obtained from

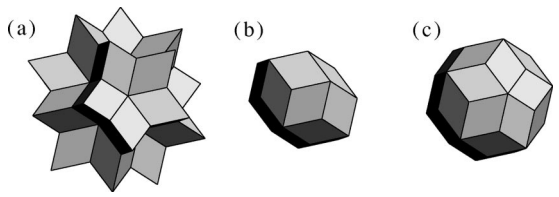

FIG. 1. The building units of the inflated 3D Penrose pattern. (a) The dodecahedral star (DS), (b) the rhombic icosahedron (RI), and (c) the rhombic triacontahedron (RT) with the edge length of a_0. They appear also as the building units of occupation domains in a higher-dimensional cluster model. In this case, the edge length is $\tau^{-3}a_0'$.

the projection of the unit cell in the 6D icosahedral lattice onto the 3D internal space.[6,38]

The OD of the 3DPP is the rhombic triacontahedron with an edge length a_0', and each edge of the triacontahedron is parallel to one of $\mathbf{d}_j^i (j \leqslant 6)$. (The superscripts e and i represent the external and internal space components of a 6D vector throughout the paper.) The 3DPP consists of two kinds of rhombohedra with an edge length a_0. An acute rhombohedron has edges parallel to $\mathbf{d}_1^e$, $\mathbf{d}_2^e$, and $\mathbf{d}_3^e$, while, an obtuse one to $\mathbf{d}_4^e$, $-\mathbf{d}_5^e$, and $\mathbf{d}_6^e$.

From the self-similarity of the icosahedral lattice, the 3DPP with $\tau^3 a_0$ ($\simeq$20 Å) edges can be obtained from a rhombic triacontahedron with an edge length of $\tau^{-3}a_0'$, where τ^3 is the similarity ratio of the primitive icosahedral lattice.[34] The real i-Al-Pd-Mn quasicrystal is face-centered and has a doubled lattice constant $a=2a_0$. We distinguish the coordinates with respect to a and a_0 by (x,y,z,t,u,v) and $(x,y,z,t,u,v)_0$. Then the same 3DPP is obtained from the rhombic triacontahedron at (0,0,0,0,0,0) and (1,0,0,0,0,0)/2 and positions equivalent to them under the centering translations. The 32 centering translations of the face-centered icosahedral lattice are given by (0,0,0,0,0,0), (1,1,0,0,0,0)/2, (1,0,1,0,0,0)/2, . . . ,(1,1,1,1,1,1)/2. The even-parity vertices of the 3DPP are generated by the OD's at (0,0,0,0,0,0) and 31 other equivalent positions, while the odd-parity ones by the OD's at (1,0,0,0,0,0)/2 and the equivalent positions.

We call the 3DPP with an edge length of $\tau^3 a_0$ an *inflated* 3DPP. The inflated 3DPP can be considered to consist of a dodecahedral star (DS), rhombic icosahedron (RI), rhombic triacontahedron (RT) and obtuse rhombohedron (OR) with an edge length of a_0 (see Fig. 1).

It is known that the DS is located at each vertex of the inflated 3DPP, the RI is at the edge center of each edge and the RT is at two positions on the body diagonal of each acute rhombohedron of the inflated 3DPP (Fig. 2).[39] Therefore we consider three kinds of clusters accommodated in these three polyhedra, which are called *cages* hereafter. The OR appears in a gap of them in the inflated OR [Fig. 2(f)].

The building units of the inflated 3DPP can be decorated based on the polyhedral occupation domains with the same shape as the building units in Fig. 1 but the length of each edge is $\tau^{-3}a_0'$. (Note that building units in Fig. 1 are the polyhedra in the external space, while OD's discussed here are those in the internal space.) For convenience, polyhedral

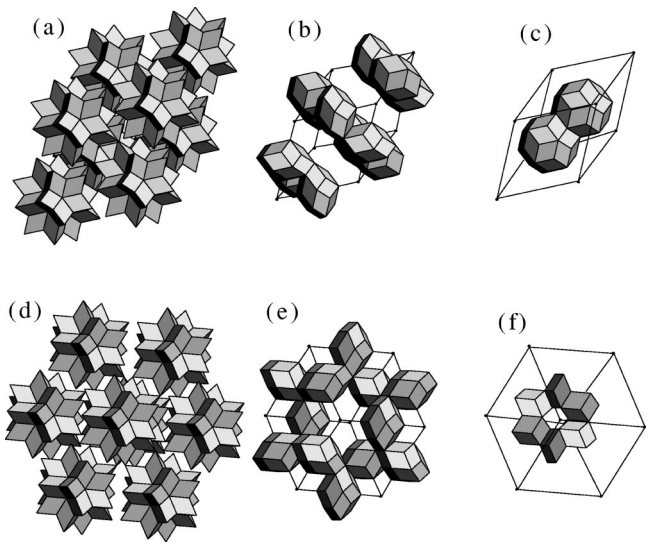

FIG. 2. The inflated rhombohedra composed of building units shown in Fig. 1. (a) The dodecahedral stars located at vertices of the inflated acute rhombohedron. (b) The rhombic icosahedra at edge centers. (c) Two rhombic triacontahedra at the body diagonal. (d) The dodecahedral stars at vertices of the inflated obtuse rhombohedron. (e) The rhombic icosahedra at the edge centers. (f) The six obtuse rhombohedra. In (c) the two rhombic triacontahedra share one obtuse rhombohedron and in (d), one acute rhombohedron is shared by two dodecahedral stars on the short diagonal of the inflated obtuse rhombohedron.

OD's with edge lengths of $\tau^{-3}a_0'$ and a_0' are hereafter called the small and large OD's. If we decorate DS, RI, and RT constituting the inflated 3DPP in a similar manner, we can obtain a clear cluster model, where the same atom clusters appear at each vertex, edge center, or two body-diagonal positions of the acute rhombohedron, although the face-centered lattice requires different clusters for the even- and odd-parity vertices. Such a model can be given on the basis of the small RT placed at (1,1,1,1,1,1)/4 and (3,1,1,1,1,1)/4 of the face-centered icosahedral lattice as shown below. (Note that there are 64 OD's related to them in the unit cell, because of the 32 centering translations.) From the self-similarity of the 3DPP, the small RT's centered at these two positions give the inflated 3DPP. The edge center of the inflated 3DPP is derived from the small RI at (1,0,0,0,0,0)/4, while the body-diagonal two positions are obtained from the small DS at the origin and (1,0,0,0,0,0)/2 as discussed in the next section.

IV. ATOM POSITIONS IN SIX-DIMENSIONAL SPACE

It is well known that the 3DPP with the edge length of a_0 is generated by the RT with the edge length of a_0' placed at the origin of the primitive icosahedral lattice.[6,38] Similarly, the edge center of the 3DPP is given by the RI at $(1,0,0,0,0,0)_0/2$ and the body-diagonal two positions of the acute rhombohedron, the DS at $(1,1,1,1,1,1)_0/2$.[40] For the corresponding sites in the inflated 3DPP is easily obtainable by the similarity transformation for the icosahedral lattice.

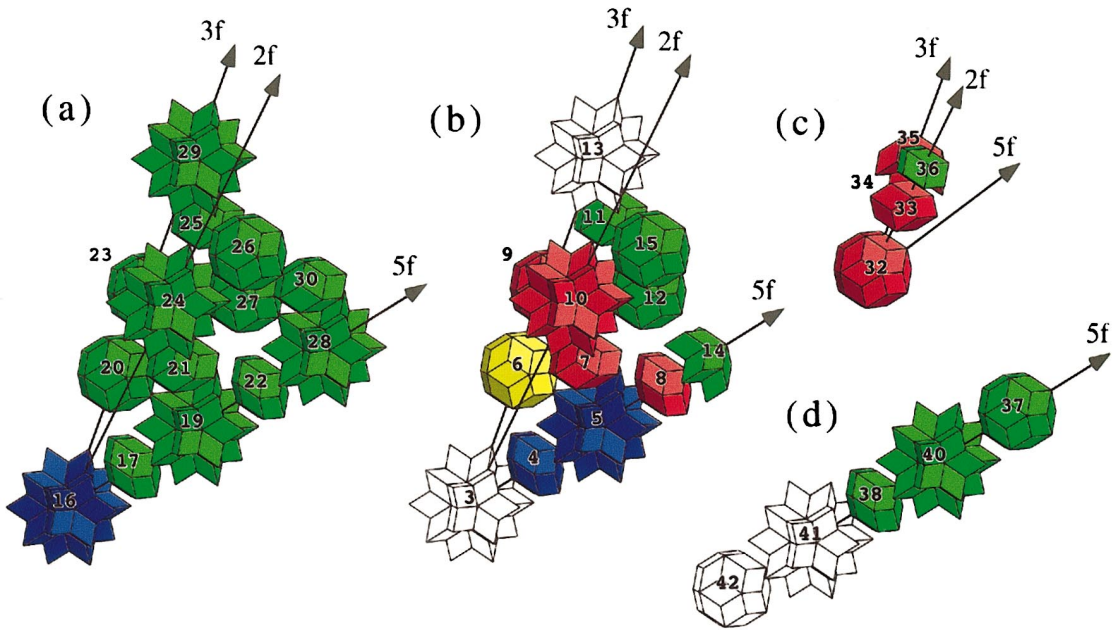

FIG. 3. (Color) The independent parts of large occupation domains at (a) (0,0,0,0,0,0), (b) (1,0,0,0,0,0)/2, (c) (3,1,1,1,1,1)/4, and (d) (1,0,0,0,0,0)/4. For visibility, a small gap is introduced between small occupation domains. The edge length of each polyhedron is $\tau^{-3}a_0'$. Domains without shading are not occupied by any atoms in *i*-Al-Pd-Mn but added for discussions (see text). Green, red, yellow, and blue OD's are assumed to be statistically occupied by Al/Mn, Pd/Mn, Mn/Al, and Mn/Pd. In each pair, the first species was expected to be predominant in the initial model of the refinement. Arrows show the fivefold (5f), threefold (3f) and twofold (2f) axes passing through the center of the large occupation domains. [Note that the OD No. 38 is at (1,0,0,0,0,0)/4 in (d).]

The similarity transformation matrix S for the face-centered icosahedral lattice is given by

$$S=\frac{1}{2}\begin{pmatrix} 1 & 1 & 1 & 1 & 1 & 1 \\ 1 & 1 & 1 & -1 & -1 & 1 \\ 1 & 1 & 1 & 1 & -1 & -1 \\ 1 & -1 & 1 & 1 & 1 & -1 \\ 1 & -1 & -1 & 1 & 1 & 1 \\ 1 & 1 & -1 & -1 & 1 & 1 \end{pmatrix}. \qquad (3)$$

On the other hand, that of the primitive icosahedral lattice is given by S^3.[34] This inflates the external component of a 6D vector by τ^3 while deflates the internal component by the factor of τ^{-3}. The three kinds of cluster centers in the inflated 3DPP mentioned above are therefore obtained from small RT, small RI, and small DS placed at $(0,0,0,0,0,0)_0$, $S^3(1,0,0,0,0,0)_0/2$, and $S^3(1,1,1,1,1,1)_0/2$ respectively. In the face-centered icosahedral lattice, these points are equivalent to (0,0,0,0,0,0), (1,0,0,0,0,0)/2, (0,1,1,1,1,1)/4, (2,1,1,1,1,1)/4, (1,1,1,1,1,1)/4, and (3,1,1,1,1,1)/4. The two positions for RI are however equivalent under the inversion. We assume inversion symmetry throughout the paper.

In the structure analysis, the origin is taken at the center of small DS. In this coordinate system, the coordinates of small RT and small DS are interchanged and those of RI are $(-1,0,0,0,0,0)/4$. The latter is equivalent to (1,0,0,0,0,0)/4 as mentioned above. We use this setting in the following.

We consider real atom positions in the cages. In the higher-dimensional cluster model, the OD's creating atoms around the cluster centers are obtained from the ODs for the centers by shifting them along the external space.[12] In a realistic model, the shifts are strongly constrained. As is clear from the electron density given by the experiments, the large OD's are observed only at (0,0,0,0,0,0), (1,0,0,0,0,0)/2, and (3,1,1,1,1,1)/4. This means that the shifted small OD's have to be a part of the large OD's. (Otherwise, many small OD's located separately are expected.)

Such a subdivision of the large OD's into small ones is achieved inversely by reconstructing the experimentally obtained OD's with small OD's. This reconstruction is practical because only rough size and shape of each large OD can be obtained from the experiment. The OD's at (0,0,0,0,0,0) and (1,0,0,0,0,0)/2 (called the OD's *A* and *B* hereafter) can be constructed mainly by the three kinds of small occupation domains shown in Fig. 1(a)–1(c). As mentioned above, the small DS's are situated at the centers of OD's *A* and *B*. For the reconstruction of the OD's *A* and *B*, we can use the connection of small OD's, which is similar to the cage connections in the external space. As shown later, this subdivision leads to the cluster appearing in the 2/1 approximant. The positions of the independent small occupation domains are shown in Figs. 3(a) and 3(b) and Table I. (Note that Table I uses the coordinate system with respect to the lattice constant a_0.)

For OD *C*, we need to consider new connection of the small OD's. This is formed by the small RT's centered at (3,1,1,1,1,1)/4 and at $(1,1,1,0,0,0)_0^i$ from it. The latter can be subdivided into two small rhombic dodecahedra (RD's) along the two-fold axis and small four acute rhombohedra

TABLE I. The positions of the independent OD's in the six-dimensional model. The first column shows the Wyckoff symbol (WS), with the number indicating the multiplicity. The second column denotes its site symmetry (SS). The position of each OD is given by $\mathbf{x}_0+\mathbf{x}^i$. The assumed atom pair and the occupation domain in Fig. 1 are listed in the fourth and fifth columns. In the fifth column, (d), (e), and (f) represent a small rhombic dodecahedron, and a small acute rhombohedron, and five acute rhombohedra, respectively (see Fig. 3). The OD is numbered in the last column. The OD's with asterisks (41 and 42) are added to the original OD's to generate some atom positions in the 1/1 crystal approximant. In Figs. 5–12, the atom pairs Al/Mn, Pd/Mn, Mn/Pd, and Mn/Al are represented by green, red, blue, and yellow, respectively. The structure refinement showed that in most cases, the first atom in each pair is predominantly occupied.

WS	SS	$\mathbf{x}^i$	Atom	OD	No.	WS	SS	$\mathbf{x}^i$	Atom	OD	No.
OD *A*		$\mathbf{x}_0=(0,0,0,0,0,0)_0$				OD *B*		$\mathbf{x}_0=(1,0,0,0,0,0)_0$			
20*a*	3*m*	$\tau^{-2}(-1,1,0,0,1,0)^i_0$	Al/Mn	(a)	20	12*a*	5*m*	$\tau^{-2}(-1,1,0,0,1,0)^i_0$	Mn/Al	(a)	6
20*a*	3*m*	$\tau^{-1}(-1,1,0,0,1,0)^i_0$	Al/Mn	(a)	23	20*a*	3*m*	$\tau^{-1}(-1,1,0,0,1,0)^i_0$	Pd/Mn	(a)	9
60*a*	2	$\tau^{-1}(-\tau,\tau,-1,0,0,0)^i_0$	Al/Mn	(a)	27	12*a*	5*m*	$(1,0,0,0,0,0)^i_0/2$	Mn/Pd	(b)	4
60*a*	2	$(-\tau^1,1,0,0,0,0)^i_0$	Al/Mn	(a)	26	60*a*	*m*	$(-1,2,0,0,0,0)^i_0/2$	Pd/Mn	(b)	7
60*a*	2	$(1,\tau^2,0,0,0,0)^i_0$	Al/Mn	(a)	31	12*a*	5*m*	$(-3,0,0,0,0,0)^i_0/2$	Pd/Mn	(b)	8
12*a*	5*m*	$(-1,0,0,0,0,0)^i_0/2$	Al/Mn	(b)	17	60*a*	*m*	$(-1,2,0,0,2,0)^i_0/2$	Al/Mn	(b)	11
60*a*	*m*	$(-1,2,0,0,0,0)^i_0/2$	Al/Mn	(b)	21	1*a*	$m\overline{35}$	$(0,0,0,0,0,0)^i_0$	Mn/Al	(c)	3
12*a*	5*m*	$(-3,0,0,0,0,0)^i_0/2$	Al/Mn	(b)	22	12*a*	5*m*	$(-1,0,0,0,0,0)^i_0$	Mn/Pd	(c)	5
60*a*	*m*	$(-1,2,0,0,2,0)^i_0/2$	Al/Mn	(b)	25	30*a*	2*mm*	$(-1,1,0,0,0,0)^i_0$	Pd/Mn	(c)	10
60*a*	*m*	$(-4,1,0,0,0,0)^i_0/2$	Al/Mn	(b)	30	20*a*	3*m*	$(-1,1,0,0,1,0)^i_0$		(c)	13
1*a*	$m\overline{35}$	$(0,0,0,0,0,0)^i_0$	Mn/Pd	(c)	16	60*a*	2	$\tau^{-1}(-\tau,\tau,-1,0,0,0)^i_0$	Al/Mn	(f)	12
12*a*	5*m*	$(-1,0,0,0,0,0)^i_0$	Al/Mn	(c)	19	20*a*	3*m*	$(-2,0,0,0,0,0)^i_0$	Al/Mn	(f)	14
12*a*	5*m*	$(-2,0,0,0,0,0)^i_0$	Al/Mn	(c)	28						
30*a*	2*mm*	$(-1,1,0,0,0,0)^i_0$	Al/Mn	(c)	24						
20*a*	3*m*	$(-1,1,0,0,1,0)^i_0$	Al/Mn	(c)	29						
OD *C*		$\mathbf{x}_0=(3,1,1,1,1,1)_0/2$				OD *D*		$\mathbf{x}_0=(1,0,0,0,0,0)_0/2$			
20*a*	3*m*	$(0,0,0,0,0,0)^i_0$	Pd/Mn	(a)	32	12*a*	5*m*	$\tau^{-3}(-5,2,2,2,2,2)^i_0/2$	Al/Mn	(a)	37
30*a*	2*mm*	$\tau^{-3}(-2,2,0,1,1,0)^i_0/2$	Pd/Mn	(d)	33	12*a*	5*m*	$(0,0,0,0,0,0)^i_0$	Al/Mn	(b)	38
20*a*	3*m*	$\tau^{-3}(-1,1,1,1,1,-1)^i_0/2$	Pd/Mn	(e)	34	12*a*	5*m*	$\tau^{-3}(-2,1,1,1,1,1)^i_0/2$	Al/Mn	(c)	40
20*a*	3*m*	$\tau^{-3}(-3,3,1,1,3,-1)^i_0/2$	Pd/Mn	(e)	35	12*a*	5*m*	$-\tau^{-3}(-2,1,1,1,1,1)^i_0/2$		(c)	41*
30*a*	2*mm*	$\tau^{-3}(-3,3,0,2,2,0)^i_0/2$	Al/Mn	(d)	36	12*a*	5*m*	$-\tau^{-3}(-5,2,2,2,2,2)^i_0/2$		(a)	42*

around the three-fold axes. [Exactly speaking, a small part of the RD in OD 36 in Fig. 3(c) has to be removed but this is neglected in this paper.] The symmetry operations create 20 interpenetrating small RT's sharing a small RD [No. 33 in Fig. 3(c)] and a part of another RD (No. 36). Each of these 20 small RT share a small obtuse rhombohedron with the central small RT (No. 32). This leads to Fig. 4(c).

During the structure refinement additional small OD's around (1,0,0,0,0,0)/4 shown in Fig. 3(d) were introduced. In the real *i*-Al-Pd-Mn, nonshaded small OD's are not occupied and the OD No. 40 is statistically occupied with a small occupation probability. It is noted that the symmetry of the occupation domain around (1,0,0,0,0,0)/4 is $5m$ in contrast to other three large OD's. This is because of the site symmetry of the OD's: the other three OD's [Figs. 4(a)–4(c)] are situated at the special position with the site symmetry of $m35$, while the former is at the special position with $5m$.

For the structure refinement, we assign a pair of atoms for each small OD together with the temperature factor and the shift from the ideal position along the external space. The occupation ratio of the second species of the pair for each OD is refined together with the total occupation probability of some atoms by the least-squares program. The assumed pair for each small OD is listed in the fourth column in Table I. The pairs Al/Mn, Pd/Mn, Mn/Al, and Mn/Pd are represented by green, red, yellow, and blue in Figs. 3 and 5–12. The Pd/Mn (red) and Mn/Pd (blue) pairs are equivalent, but for all pairs including these two, the first species was as-

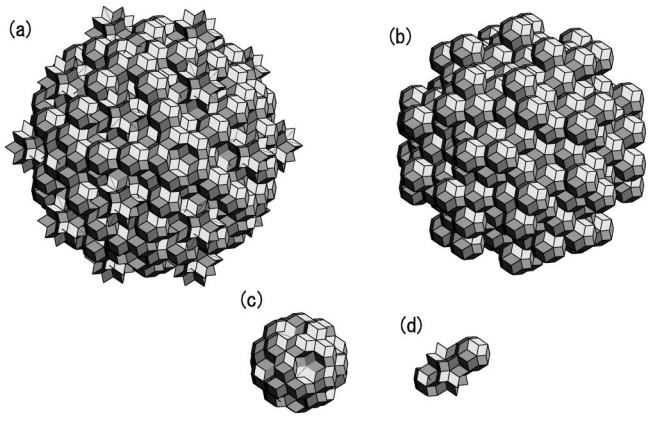

FIG. 4. The total occupation domains used in the refinement of *i*-Al-Pd-Mn. (a) the occupation domain *A* at (0,0,0,0,0,0), (b) *B* at (1,0,0,0,0,0)/2, (c) *C* at (3,1,1,1,1,1)/4, and (d) *D* at (1,0,0,0,0,0)/4. The unoccupied OD's shown as unshaded polyhedra in Fig. 3 are not written.

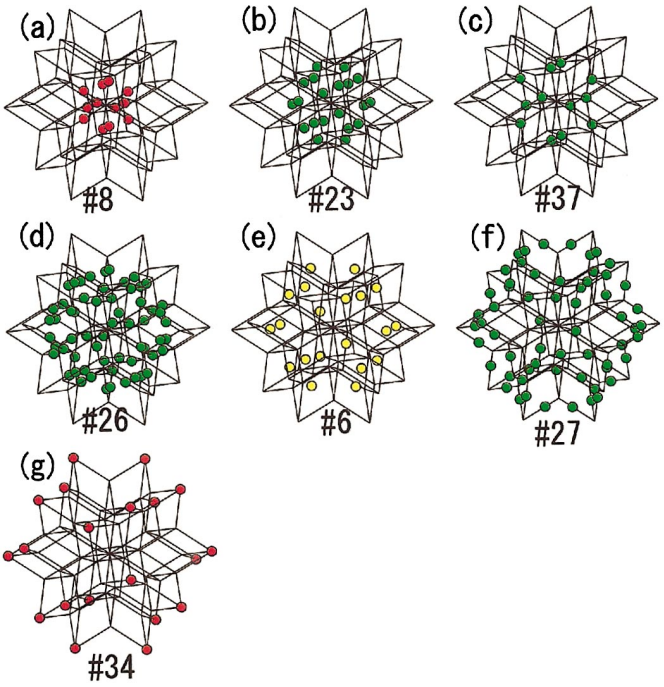

FIG. 5. (Color) The decoration of the dodecahedral star in Fig. 2 located at the even-parity vertices of the inflated 3DPP (green, Al/Mn; red, Pd/Mn; blue, Mn/Pd; yellow, Mn/Al).

sumed to be predominant in the initial model for the refinement. The final result of the refinement proved that this assumption is correct for most OD's.

The whole domains are obtained from the independent parts shown in Fig. 3 by symmetry operations. The large OD's *A*, *B*, *C*, and *D* occupied by atoms are shown in Fig. 4. For OD shown in Fig. 3(d), the center (OD No. 38) is on the fivefold axis and the same OD's in shape but with different orientations are located at 12 equivalent positions. They are isolated from each other and from OD's *A*, *B*, and *C*.

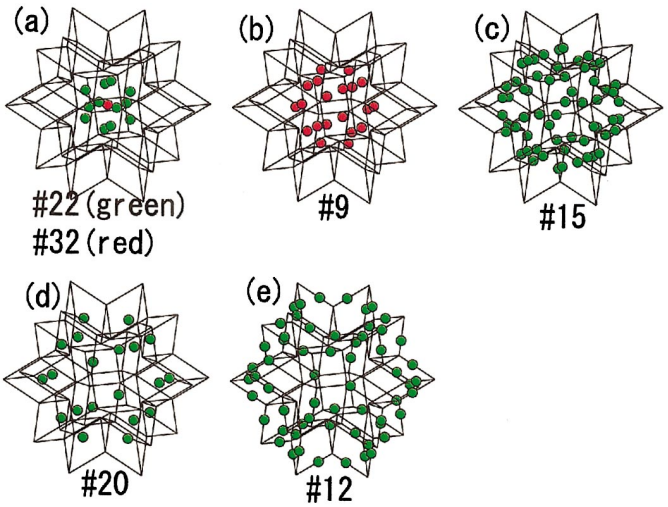

FIG. 6. (Color) The decoration of the dodecahedral star in Fig. 2 located at the odd-parity vertices of the inflated 3DPP (green, Al/Mn; red, Pd/Mn; blue, Mn/Pd).

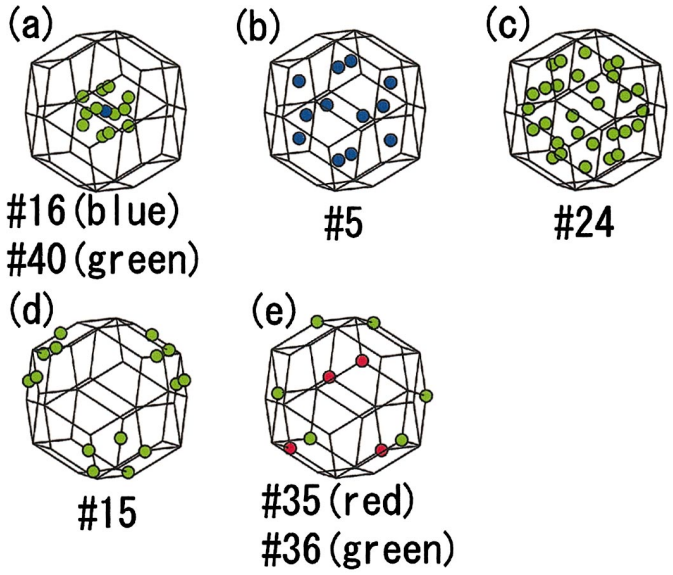

FIG. 7. (Color) The decoration of the rhombic triacontahedron in Fig. 2 located on the body-diagonal of the inflated 3DPP (green, Al/Mn; red, Pd/Mn; blue, Mn/Pd).

From the constraint of the nearest-neighbor distances, the OD's at the origin and $(-2,1,1,1,1,1)/2$ cannot overlap when they are projected into the internal space. Similarly the OD *B* at $(0,1,1,1,1,1)/2$ cannot overlap with the OD *C* at $(3,1,1,1,1,1,1)/4$. These closeness conditions are fulfilled in the present model. This 6D model gives the point density of 0.0628 $Å^{-3}$, which is comparable with the value of 0.063 $Å^{-3}$ obtained from the refinement of the 2/1 crystal approximant.[32]

In the structure refinement, we assume the same temperature factor, occupation probability, and shift of atoms within

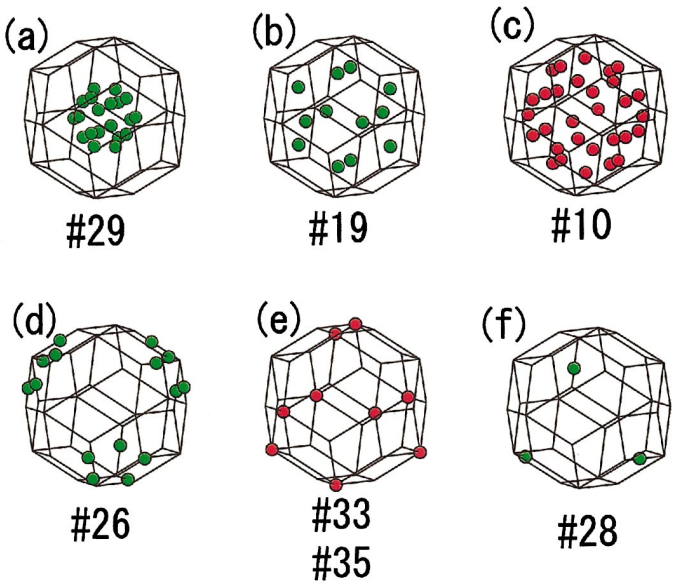

FIG. 8. (Color) The decoration of another rhombic triacontahedron in Fig. 2 located on the body-diagonal of the inflated 3DPP (green, Al/Mn; red, Pd/Mn).

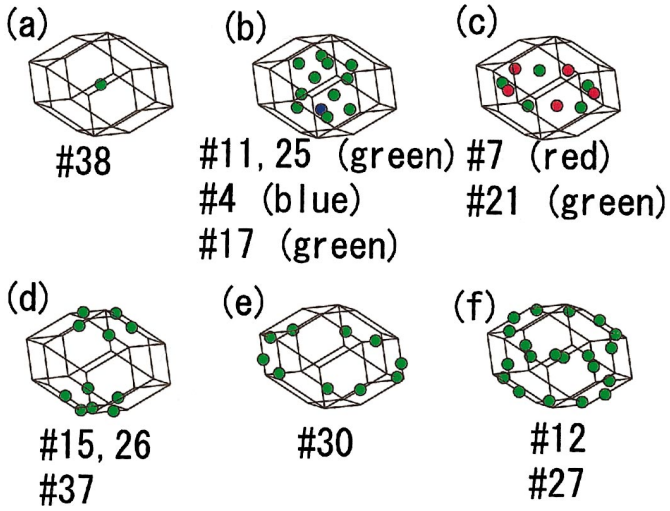

FIG. 9. (Color) The decoration of the rhombic icosahedron in Fig. 2 located at the edge center of the inflated 3DPP (green, Al/Mn; red, Pd/Mn; blue, Mn/Pd). In (b) and (d), the OD's 4, 7, and 37 are on the fivefold axis of the RI.

each small OD. This implies that each small OD plays the role of an independent atom in usual crystals, for which the coordinate, temperature factor, and occupation probability are given. Therefore the number of parameters is limited by the number of small independent OD's. For the temperature factor, we can consider the anisotropic temperature factor as well as the isotropic factor as in crystals. It is essentially important for obtaining small R factors to introduce the shift of small OD's from the ideal positions along the external space. This enables the relaxation of atom positions within the clusters, although the cluster centers are still at the ideal positions and the symmetry of the cluster maintains that of the site symmetry of the corresponding cluster center.

V. ATOM POSITIONS IN THREE-DIMENSIONAL SPACE

The OD's described in the preceding section give a clear model, which has three-atom clusters at the vertex of the inflated 3DPP, its edge center, and two body-diagonal positions of the acute rhombohedra, respectively. They are accommodated in the corresponding cages described in Sec. III. As mentioned in Sec. IV, the center of the cages are generated by the small RT, RI, and DS and their decorated atom positions are obtained from the small OD's with the same shape. The atom positions of a cluster around each cluster center can be obtained from the 3D cut passing through the center of the small OD that generates the cluster center. Therefore, the clusters in the DS cages are given by the 3D cuts passing through (1,1,1,1,1,1)/4 and (3,1,1,1,1,1)/4 (Figs. 5 and 6). These two cuts give different structures because (1,1,1,1,1,1)/4 and (3,1,1,1,1,1)/4 are not equivalent in the face-centered icosahedral lattice. Similarly, the atom arrangement in the RT cage is obtained by the cuts through (0,0,0,0,0,0) and (1,0,0,0,0,0)/2 (Figs. 7 and 8). The cluster in the RI cages is only one, but has a polarity. This is obtained from a 3D cut through (1,0,0,0,0,0)/4 (Fig. 9). Note that there is no occupation domain at (1,1,1,1,1,1)/4. This means that no atom is located at one of the DS cage centers [See Fig. 5(a)].

As is easily seen from Fig. 3, the atom positions in the DS cages are obtained from OD's 32, 6, 9, 12, 15, 20, 23, 26, 27, 37, and 42 ^{No} (the No superscript means that these OD's are

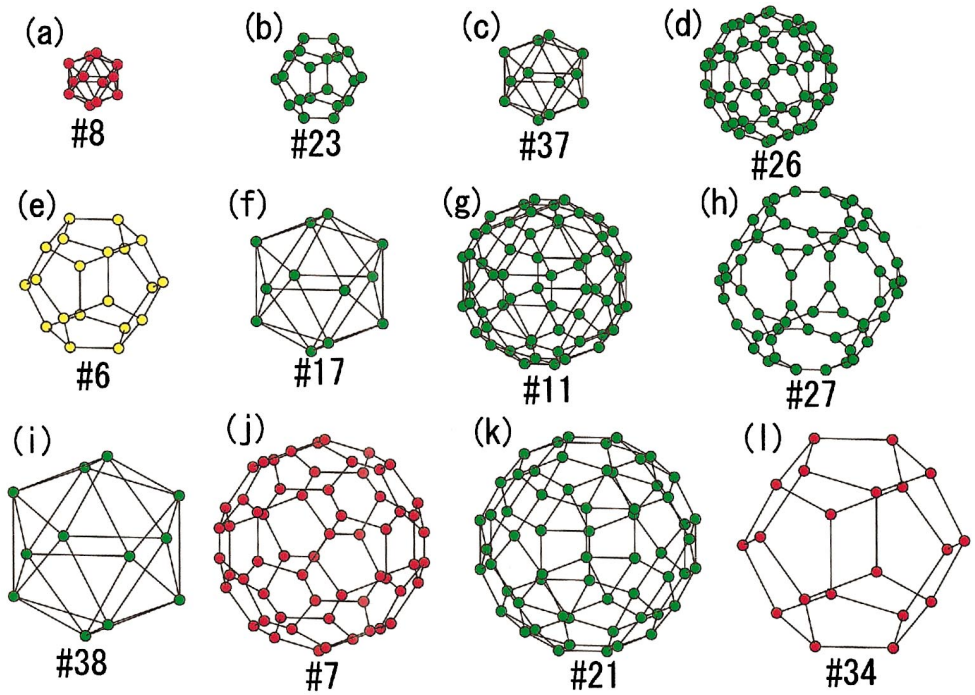

FIG. 10. (Color) The 12 shells (a)–(l) of the 20 Å clusters at (1,1,1,1,1,1)/4. These shells are essentially the same as those in β-Al-Pd-Mn-Si (green, Al/Mn; red, Pd/Mn; yellow, Mn/Al).

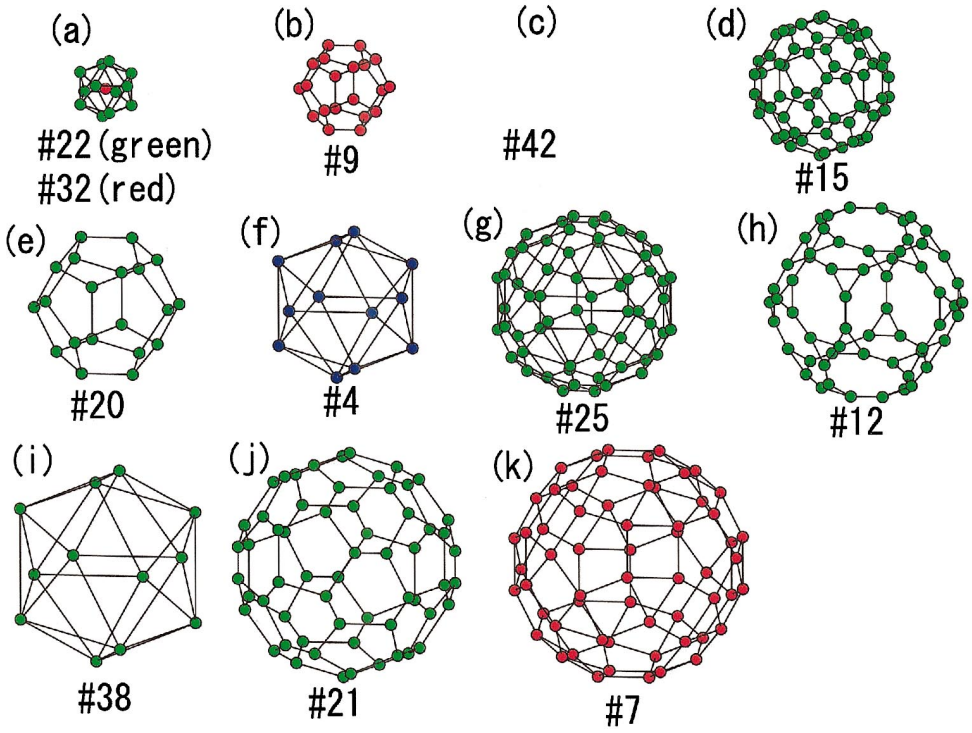

FIG. 11. (Color) The 11 shells (a)–(k) of another 20 Å cluster at (3,1,1,1,1,1)/4. This cluster does not appear in β-Al-Pd-Mn-Si but is essential for a face-centered *i*-Al-Pd-Mn. In (a), the cluster center is obtained from the OD No. 32, while other 12 are from the OD No. 22 (green, Al/Mn; red, Pd/Mn; blue, Mn/Pd).

not occupied by atoms) (Figs. 5 and 6). Similarly, the atom positions in the RT cages are generated by OD's 3^{No}, 5, 10, 13^{No}, 16, 19, 24, 29, and 41^{No}, while those in the RI cages are given by OD's 4, 7, 11, 17, 21, 25, 30, and 38. (Figs. 7–9). The OD 28 gives 12 sites on the fivefold axis of the RT at the distance $2a_0$ from the center of the RT shown in Fig. 7 but they are out of the RT. They are not drawn in Fig. 7. The OD's 8 and 22 create the sites on the fivefold axis of the RI but they are out of the RI. They appear in the DS cages because the RI cage is located between two DS cages. [Figs. 5(a) and 6(a)]. For the same reason, the sites on the surface of the DS cages are on the surface of the RI cages. Such sites are shown in Figs. 7(d) and 8(d).

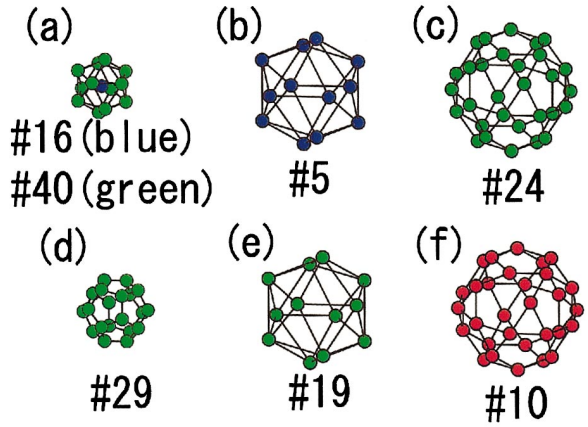

FIG. 12. (Color) Two Mackay-like clusters (a)–(c) and (d)–(f), which are located at the body-diagonal two positions of the acute rhombohedron in 3DPP (green, Al/Mn; red, Pd/Mn; blue, Mn/Pd).

The atom positions out of the cages mentioned here are in some cases in another cage. For example, OD's 8 and 22 create the first shells of the cluster in the RD cages [Figs. 5(a) and 6(a)]. These positions are created by small RT's located at $\tau a_0'$ from the center of the large OD's shown in Figs. 3(b) and 3(a). In the former, the RT's consist of the OD's 8 and 14 and a part of the OD 12 (a small obtuse rhombohedron). Similarly, it is composed of the OD 22 and parts of the OD's 27 and 28 in the latter. The some atom sites created by the OD 28 are located at the surface of another RT as shown in Fig. 8(f).

The OD's 33, 34, 35, and 36 (and a small part of OD 32) form the 20 RT's on the threefold axes around OD 32, which are interpenetrated [see Fig. 4(c)]. These OD's generate atoms at the tips of the DS cages located at the even-parity vertices of the inflated 3DPP. [Fig. 5(g)]. As a result in the DS at the even-parity vertex of the inflated 3DPP, the atoms are at every tip on the threefold axis. This leads to the decoration which is shown in Fig. 5. On the other hand, no such atoms are present for the DS at the odd-parity vertex (Fig. 6).

It should be noted that the decoration of the RT in Figs. 7 and 8 has a three-fold symmetry, reflecting the point symmetry of the center of the RT in the inflated 3DPP. Similarly, the decoration of RI is of fivefold-symmetric. The structure refinement, however, showed that the OD's with No superscripts are not occupied by atoms. They are added for discussion later in this section.

The decoration of each cage determines the whole 3D

structure of *i*-Al-Pd-Mn since the locations of these cages in the inflated 3DPP are known. There are 24 types of vertices with different neighbors in the (inflated) 3DPP[6,38] and their frequency is known.[41] Each vertex is a point from which several edges along the fivefold axes go out or is a common point over several acute and obtuse rhombohedra with face to face contact. The number of edges going out or the direction of the edges is different depending on the types of vertices. The local symmetry of the vertex is generally different because of different edge arrangements. We will discuss some typical features of the present model that are due to the arrangement of cages in the inflated 3DPP. As a result of the arrangement of the edges of the inflated 3DPP, there exist large icosahedral clusters at the even- and odd-parity 12-fold vertices of the inflated 3DPP. There are 12 RI cages on the fivefold axes around the DS cage at the 12-fold vertex. (Note that a RI cage is situated at each edge center of the inflated 3DPP.) These clusters are about 20 Å in diameter (which is equal to $\tau^3 a_0$). They consist of 12 or 11 shells as shown in Figs. 10 and 11. One of these clusters (Fig. 10) is quite similar to the 20 Å cluster in the 2/1 approximant of *i*-Al-Pd-Mn, that is, β-Al-Pd-Mn-Si.[29,32] Both clusters consist of similar shells. This suggests that the present model is reliable and the structure refinement based on the model will be successful if the 2/1 approximant has a local environment similar to that of *i*-Al-Pd-Mn.

Other small icosahedral clusters are located at the RT on the two body-diagonal positions of each inflated acute rhombohedra in the inflated 3DPP [Fig. 2(c)]. They are shown in Fig. 12. The first shells of the clusters are generated by the OD's 29 and 40. The OD 29 causes 20 atom positions, with a short interatomic distance ($\simeq$1.8 Å), so that they have to be occupied statistically with an occupation probability less than 0.5. On the other hand, the OD 40 gives 12 atom sites forming a regular icosahedron with a reasonable interatomic distance ($a_0/2 \simeq 2.3$ Å). This means that the same icosahedral shell may be considered in *i*-Al-Pd-Mn. If we use OD 41 instead of OD 29, we get such a cluster. In this case, the both clusters are quite similar to the so-called Mackay cluster. However, the structure refinement showed that one of the two is highly disordered and is statistically occupied.

A very small icosahedral cluster appearing at the center of the DS cages shown in Fig. 6(a) also appears at each tip of the DS cages shown in Fig. 5(g). This is due to the shape of the total OD at the origin or (1,1,1,1,1,1)/2 (OD *A*) as explained below. (The OD's at these two positions are the same because the lattice is face-centered.) For the former, the cluster center is given by the OD 32, while that of the latter is generated by the rest of the total OD (OD *C*) at (3,1,1,1,1,1)/4 [Fig. 4(c)]. The atoms of the first shell are on the fivefold axes and are distant from the center by $\tau^{-1}a_0$. The distances between (1,1,1,1,1,1)/2 and (3,1,1,1,1,1)/4 in the external and internal spaces are $\tau^{-1}a_0$ and $\tau a_0'$. When the OD *C* is projected onto the internal space passing through (1,1,1,1,1,1)/2, the center comes to the point on the fivefold axis with the distance $\tau a_0'$ from the center of the OD *A* and the projected OD *C* is completely included in the OD *A* distance. This ensures that around every site created by the OD *C*, there are 12 atom sites forming an icosahedron with the radius of $\tau^{-1}a_0$, which are generated by the corresponding parts of the 12 OD's (OD *A*) around the OD *C*. (Note that the site symmetry of the center of the OD *C* is the icosahedral $m\bar{3}5$.) There exist such clusters in the 2/1 approximant. The cluster centers are the atoms in the 12th shell of the 20 Å cluster, which correspond to the atom positions in Figs. 5(g) or 10(l). (See Fig. 5 in Ref. 42.) The 12 atom positions in each small cluster are generated by OD's 21, 24, 27, and 28.

VI. LINEAR PHASON IN ICOSAHEDRAL QUASICRYSTALS

As is well known, the crystal approximant structure can be obtained from a 6D model by introducing linear phason strain. This is specified by the strain tensor shown below. When the unit vectors of the distorted lattice are given by

$$\mathbf{d}_i' = \sum_{j=1}^{6} Q_{ij}\mathbf{a}_j' = \sum_{j=1}^{6} (QT)_{ij}\mathbf{a}_j, \tag{4}$$

T gives the strain tensor for the linear phason strain, which has the following form:

$$T = \begin{pmatrix} I_3 & U \\ 0 & I_3 \end{pmatrix}, \tag{5}$$

where I_3 is a 3×3 unit matrix and U is a general 3×3 matrix.

It is convenient to use two sets of unit vectors of the external and internal spaces. Pentagonal, cubic, and trigonal quasicrystals can be derived from the icosahedral quasicrystals, as shown by Ishii.[43] (In the usual sense, the definition of the quasicrystal excludes a structure with a crystallographic point group. We call, however, an aperiodic structure obtained from a quasicrystal with noncrystallographic point group by a linear phason strain a quasicrystal for convenience.) For pentagonal quasicrystals, $\mathbf{a}_i (i=1,2,\ldots,6)$ given by Eq. (1) are convenient but another unit vector set is more appropriate for the latter two, although both sets can express all possible distortions. This is because two axes $\mathbf{a}_3$ and $\mathbf{a}_6$ are parallel to the fivefold axis in Eq. (1). Then nonzero $U_{11}=U_{22}$ and U_{33} give the pentagonal quasicrystals. In order to treat the latter two cases, it is convenient to take unit vectors $\mathbf{a}_j^c$ parallel to the twofold axes,[40] which are defined by $\mathbf{d}_i = \Sigma_{j=1}^{6} Q_{ij}^c \mathbf{a}_j^c$ with

$$Q^c = \frac{a_0}{\sqrt{2+\tau}} \begin{pmatrix} 1 & \tau & 0 & \tau & -1 & 0 \\ \tau & 0 & 1 & -1 & 0 & \tau \\ \tau & 0 & -1 & -1 & 0 & -\tau \\ 0 & 1 & -\tau & 0 & \tau & 1 \\ -1 & \tau & 0 & -\tau & -1 & 0 \\ 0 & 1 & \tau & 0 & \tau & -1 \end{pmatrix}. \tag{6}$$

The phason strain matrix T in this setting is defined in Eq. (4) by replacing $\mathbf{a}_i$ with $\mathbf{a}_i^c$ and Q_{ij} with Q_{ij}^c. Then nonzero $U_{11}=U_{22}=U_{33}$ gives cubic quasicrystals and $U_{12}=U_{23}$

$=U_{31}$ and $U_{13}=U_{21}=U_{32}$ lead to trigonal quasicrystals. Such a quasicrystal with a crystallographic point group becomes a crystal in a particular case as shown in the next section.

VII. 2/1 CUBIC CRYSTALLINE APPROXIMANTS

Crystalline approximants are obtained when three linearly independent 6D lattice points are on the 3D external space passing through the origin. The coordinates z_i with respect to $\mathbf{a}_i^c$ of the lattice vector $\mathbf{n}=\Sigma_{j=1}^{6} n_j \mathbf{d}_j'$ are given by

$$z_i=\sum_{j=1}^{6} (\tilde{T}\tilde{Q}^c)_{ij} n_j, \tag{7}$$

where the tilde means the transpose. From the condition under which the internal space components are zero, we can obtain the strength of the phason strain. Let the origin and the three points $\mathbf{n}^1$, $\mathbf{n}^2$, $\mathbf{n}^3$ be on the external space. Then the nine internal space components of the three lattice vectors $\mathbf{n}^1$, $\mathbf{n}^2$, $\mathbf{n}^3$ should be zero. This determines the nine matrix elements of the 3×3 matrix U. The condition can be expressed in the matrix form, $\tilde{U}RN+SN=O$, where R and S are the upper and lower 3×6 matrices of $\tilde{Q}^c$, O is a 3×3 zero matrix, and N is a 6×3 matrix $(\mathbf{n}^1,\mathbf{n}^2,\mathbf{n}^3)$. Thus the matrix $\tilde{U}$ is given by

$$\tilde{U}=-(SN)(RN)^{-1}. \tag{8}$$

In the case of the 2/1 cubic approximant, the external space passes through the origin and $\mathbf{n}_1=(1,2,2,0,\bar{1},0)'$, $\mathbf{n}_2=(2,0,0,1,2,1)'$, and $\mathbf{n}_3=(0,1,\bar{1},\bar{2},0,2)'$, where the prime means coordinates with respect to the deformed unit vectors $\mathbf{d}_i'$. Therefore if they are the unit vectors in the crystalline approximant, their internal components are zero. Then from Eq. (8) we have $U_{11}=U_{22}=U_{33}=\tau^{-5}$ and $U_{ij}=0$ for $i\neq j$.[40] Similarly, for the 1/1 approximant structures, we have $\mathbf{n}_1=(1,1,1,0,\bar{1},0)'$, $\mathbf{n}_2=(1,0,0,1,1,1)'$, and $\mathbf{n}_3=(0,1,\bar{1},\bar{1},0,1)'$. This leads to $U_{11}=U_{22}=U_{33}=-\tau^{-3}$. It is easy to show that for the cubic approximant represented by consecutive Fibonacci numbers F_{n+1}/F_n ($F_0=0$, $F_1=1$, $F_n=F_{n-2}+F_{n-1}$ for $n>1$) the nonzero matrix elements are $U_{11}=U_{22}=U_{33}=-(-1)^n\tau^{-3-2n}$ ($n\geqslant1$).

Even if we fix the period, we will obtain a different crystalline approximant structure with different symmetries by choosing the external space passing through a different position in the 6D space.[44] In general the symmetry of the approximant is equal to that of the special position with the highest symmetry on the 3D hyperplane and the cubic approximants are obtained from the 3D hyperplane passing through 6D points with the point symmetry $m\bar{3}5$. The other special positions have a symmetry equal to $5m$ or lower than $m\bar{3}$ and the former point group is not a supergroup of the cubic point group $m\bar{3}$. Therefore we need to choose a 3D hyperplane passing through the points with $m\bar{3}5$ symmetry under no phason strain in order to obtain a cubic approximant. (We consider approximants with a symmorphic space group. For the case of nonsymmorphic space groups such as $Pa\bar{3}$, we need different considerations.) There are four such points in the face-centered icosahedral lattice: $(0,0,0,0,0,0)'$, $(1,0,0,0,0,0)'/2$, $(1,1,1,1,1,1)'/4$, and $(3,1,1,1,1,1)'/4$. Among them, the hyperplane passing through $(1,1,1,1,1,1)'/4$ gives the structure corresponding to the real 1/1 and 2/1 approximant structures (α- and β-Al-Pd-Mn-Si).

The model given by the OD's in Fig. 3 gives a 2/1 crystal approximant structure, which is essentially the same as the real approximant. As shown by Sugiyama *et al.*,[32] the approximant consists of 20 Å clusters that can be well described by 12 shells. The shells of the calculated 2/1 approximant are the same as those in Fig. 10. The 12 shells agree well with those of the 2/1 approximant structure determined recently (see Fig. 1 of Ref. 32). The cluster center of this model is empty as in the approximant. The nearest interatomic distance of the fourth shell in Figs. 10 and 11, one of them coming from a part of OD 15 and the other from OD 26, are $\tau^{-2}a_0\simeq1.7$ Å. These sites should be statistically occupied as in the 2/1 approximant. These distance may be relaxed by the shifts of OD's 15 and 26 from the ideal positions along the external space.

β-Al-Pd-Mn has a slightly different small cluster around the body center, which is not reproduced from the 6D model. The Mackay icosahedron is situated in the calculated approximant, which is the same as in Figs. 12(a)–12(c), while in β-Al-Pd-Mn-Si, the first shell has a different structure and some atoms in the third shell in Fig. 12(c) are missing. Consequently the Mackay icosahedron is broken in the real approximant.

VIII. 1/1 CUBIC CRYSTALLINE APPROXIMANTS

The 1/1 approximants have larger phason distortion than the 2/1 approximants discussed in the preceding section. So the derivation of this structure from the 6D model is more challenging. Figure 13 gives the shell structures of the 1/1 approximant given by the 3D hyperplane passing through $(1,1,1,1,1,1)'/4$. They are quite similar to those of the α-Al-Pd-Mn-Si except for several shells. The shell structures of the cluster at the origin are similar to those of the inner shells of the β-Al-Pd-Mn-Si except for the fourth shell, where 24 of 60 atoms appear in the 1/1 approximant. On the other hand, the cluster at the body center is completely different. In the 2/1 approximant, the cluster is the so-called Mackay icosahedron as mentioned in the preceding section, while it is rather similar to the cluster at the origin in the 1/1 approximant. In particular, the second shell is part of the second shell at the origin. This is because the 3D hyperplane used passes through $(1,1,1,1,1,1)'/4$ in both cases and at the same time through the point equivalent to $(0,0,0,0,0,0)$ in the 2/1 approximant but through $(3,1,1,1,1,1)'/4$ in the 1/1 approximant. The OD 16 at the origin generates the center of the Mackay icosahedron in i-Al-Pd-Mn. On the other hand, the OD 32 at $(3,1,1,1,1,1)/4$ creates the center of the cluster at the odd-parity vertex of the inflated 3DPP. Therefore the inner shells in Fig. 11 appear at the body center of the 1/1 approximant.

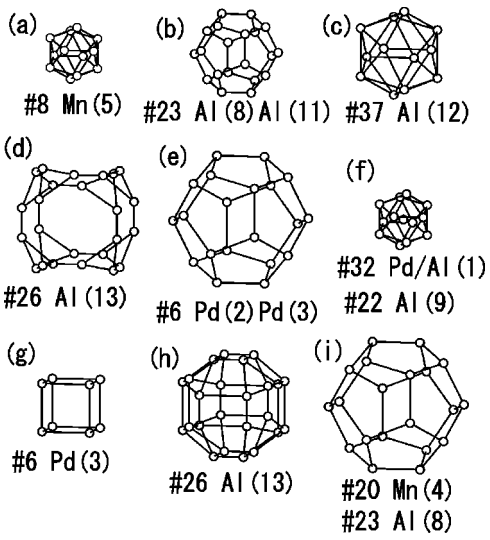

FIG. 13. The five shells (a)–(e) of the cluster located at the origin in the 1/1 approximant structure obtained from the 6D model and four shells at the body center. (f)–(i). In (f), the OD No. 32 generates the center of the cluster, while the OD No. 22, generates the other 12 sites. Atoms in the 1/1 approximants, α-Al-Pd-Mn-Si, in each shell are also shown.

IX. DISCUSSION

As shown in a separate paper,[15] the structure refinement based on the present model could explain the diffraction intensity very well. The model is a cluster-based model. The existence of clusters in quasicrystals is confirmed by the observation by high-resolution transmission electron microscopy (HRTEM). In particular, it is evident in decagonal quasicrystals. Although the projection along nonperiodic directions obscures it for icosahedral cases and it is impossible to verify only from the HRTEM images whether the observed clusters are the same or not, we can expect that a dense packing of stable clusters will stabilize the formation of quasicrystals.

The present 6D model is constructed so as to fulfill several conditions imposed by experimental results. (1) the cluster in the 2/1 approximant should be reproduced from the 6D model by the introduction of appropriate linear phason strain.[29] (2) The electron density map obtained from the low-density elimination method should be consistent with the OD's used. (3) The point density of the quasicrystal is similarly equal to that of the 2/1 approximant or the real quasicrystal.

The condition (1) can be fulfilled if we employ a higher-dimensional cluster model.[12] In order to get the 20 Å cluster, it is assumed, in the construction of the model, that the 20 Å cluster observed in the 2/1 approximant[32] is situated at each even-parity 12-fold vertex of the inflated 3DPP. In the higher-dimensional cluster model, large OD's are constructed by simple OD-generating cluster centers. However, the construction process leads to complicated large OD's at the same time. In the present case, we assumed five clusters, which are located at the even- and odd-parity vertices of the inflated 3DPP, its edge centers and the two body-diagonal positions of the acute rhombohedra of the inflated 3DPP as mentioned in Secs. III–V. This leads to the 20 Å cluster located at the even-parity 12-fold vertices. This is one of prominent features of the present model and differs from the clusters in other models where 5 Å (smaller by τ^{-3}) clusters are considered.[45–48] The 20 Å cluster is observed only in the 2/1 approximant of *i*-Al-Pd-Mn, which has the space group $Pm\bar{3}$. The 2/1 approximants for other quasicrystals found so far consist of 5 Å clusters and has the space group $Pa\bar{3}$,[33,49] as predicted from the canonical cell tiling.[45] Therefore it is reasonable to consider that *i*-Al-Pd-Mn is composed of the 20 Å clusters.

Condition (2) gives a restraint for the rough volume of the large OD's because the electron density map cannot provide a fine shape of the OD's. However, this is helpful to construct a model. Condition (3) just restrains the total volume of the OD's.[3]

We compare the present model with the model proposed by Katz and Gratias (KG) model,[24] which consists of three OD's with simple shape. In the latter, it is known that there exist many kinds of clusters with several different symmetries and a few of them have icosahedral symmetry. This is due to the fact that the large OD's have simple shape. In contrast, the present model has complicated large OD's, which are shown in Fig. 4. They generate only five clusters that pack total 3D space without large vacancies, and as a result of the arrangement of these clusters, the observed 20 Å cluster is formed at every even-parity 12-fold vertex as demonstrated in Sec. V. Therefore the difference in the shape of the large OD's causes the difference in the kinds of clusters and their symmetry. It seems to be natural that we consider the clusters observed in the approximants to be energetically stable. Then the dense packing of such clusters will stabilize the quasicrystal. On the other hand, the KG model gives another quasicrystal structure composed of many low-symmetry clusters without random phasons. The reason for the existence of such lower-symmetry clusters is not easily conceivable. For this reason we employed the higher-dimensional cluster model in our analysis.

We introduced an OD with the point symmetry $5m$ [Fig. 4(d)] which is located at (1,0,0,0,0,0)/4. In the model used in the refinement, OD's 37 and 40 are placed on the fivefold axis around the odd-parity body center. [See Fig. 1(c) in Ref. 15.] In this paper, they are shifted along the fivefold direction in the external space by $(0.5-\tau^{-1})a_0 \simeq 0.5$ Å. Then the shifted OD's are on the fivefold axis at (1,0,0,0,0,0)/4, which is shown in Fig. 3(d). These two models are equivalent because the difference exists only in the position of OD's in the external space, and both models will lead to the same final structure with the refinement of the shift parameters. The position of OD 40 in Ref. 15 gives too short an interatomic distance for the innermost shell of the Mackay cluster [see Fig. 12(a)]. This is improved in the present model. The OD's corresponding to 37, 38, and 40 are not present in the KG model but OD 38 is necessary to generate atom positions in the ninth shell of the cluster in the 2/1 approximant [Fig. 10(i)]. (It should be noted that the constraint condition imposed for each OD is that its shape should have the symmetry given by its site symmetry, that is, $5m$ in this case.)

In real quasicrystals, the random phason always exists and because of the random phason, it may be difficult to distinguish one model from the other since this weakens the diffraction intensity with a diffraction vector having a large internal space components. As a result, many such reflections cannot be observed. On the other hand, a large intensity difference between these models can be expected in such reflections.

The present model was able to explain the diffraction intensities of *i*-Al-Pd-Mn. A detailed analysis of *i*-Al-Pd-Mn (or *i*-Al-Cu-Fe) based on the KG model has not been performed yet. Therefore the direct comparison is impossible at the moment. In order to obtain a detailed structure from the structure refinement based on diffraction experiments, subdivisions of large OD's as employed in the present model are necessary for introducing different atom shifts from the ideal position, temperature factor, and occupation probability for atoms in different local environments. The KG model has simple OD's but the subdivisions based on the different local atom environments are not simpler than the present ones.[48] This suggests that the use of complicated subdivisions is not avoidable for a detailed structure refinement of quasicrystals.

X. SUMMARY

This paper described in detail a 6D model structure that is based on a higher-dimensional cluster model and an electron density of *i*-Al-Pd-Mn obtained from an x-ray analysis. The model was shown to be consistent with the 2/1 approximant structure of *i*-Al-Pd-Mn, and β-Al-Pd-Mn-Si. The 1/1 and 2/1 approximant structures calculated from the 6D model by the introduction of the linear phason strain were shown and compared with the structures of α- and β-Al-Pd-Mn-Si.

ACKNOWLEDGMENT

This work was partially supported by ''Solution-Oriented Research for Science and Technology.''

[1] D. Shechtman, I. Blech, D. Gratias, and J.W. Cahn, Phys. Rev. Lett. **53**, 1951 (1984).
[2] W. Steurer, Z. Kristallogr. **190**, 179 (1990).
[3] A. Yamamoto, Acta Crystallogr., Sect. A: Found. Crystallogr. **52**, 509 (1996).
[4] A.P. Tsai, A. Inoue, and T. Masumoto, Jpn. J. Appl. Phys., Part 2 **26**, L1505 (1987).
[5] N.G.D. Bruijn, Proc. Nederl. Acad. Wetensch. Ser. A, 39–66 (1981).
[6] M. Duneau and A. Katz, Phys. Rev. Lett. **54**, 2688 (1985).
[7] T. Janssen, Acta Crystallogr., Sect. A: Found. Crystallogr. **42**, 261 (1986).
[8] C. Janot, M.D. Boissieu, J.M. Dubois, and J. Pannetier, J. Phys.: Condens. Matter **1**, 1029 (1989).
[9] W. Steurer, J. Phys.: Condens. Matter **3**, 3397 (1991).
[10] M. Boudard, M.D. Boissieu, C. Janot, G. Heger, C. Beeli, H.-U. Nissen, H. Vincent, R. Ibberson, M. Audier, and J.M. Dubois, J. Phys.: Condens. Matter **4**, 10149 (1992).
[11] M. Boudard, M.D. Boissieu, C. Janot, G. Heger, C. Beeli, H.-U. Nissen, H. Vincent, R. Ibberson, M. Audier, and J.M. Dubois, J. Non-Cryst. Solids **153&154**, 5 (1993).
[12] A. Yamamoto and K. Hiraga, Phys. Rev. B **37**, 6207 (1988).
[13] S. Weber and A. Yamamoto, Acta Crystallogr., Sect. A: Found. Crystallogr. **54**, 997 (1998).
[14] H. Takakura, A. Yamamoto, and A.P. Tsai, Acta Crystallogr., Sect. A: Found. Crystallogr. **57**, 576 (2001).
[15] A. Yamamoto, H. Takakura, and A.P. Tsai, J. Alloys Compd. **342**, 159 (2002).
[16] P. Sainfort and B. Dubost, J. Phys. (Paris), Colloq. **47**, C3 (1986).
[17] S.V. Smaalen, Phys. Rev. B **39**, 5850 (1989).
[18] T. Ishimasa, Philos. Mag. Lett. **71**, 65 (1995).
[19] J.Q. Guo, E. Abe, and A.P. Tasi, Phys. Rev. B **62**, R14 605 (2000).
[20] Y. Kaneko, Y. Arichika, and T. Ishimasa, Philos. Mag. Lett. **81**, 777 (2001).
[21] M.D. Boissieu, C. Janot, and J.M. Dubois, J. Phys.: Condens. Matter **2**, 2499 (1990).
[22] M. Cornier-Quiquandon, A. Quivy, S. Lefebvre, G. Elkaim, E. Heger, A. Katz, and D. Gratias, Phys. Rev. B **44**, 2071 (1991).
[23] C. Janot, M. De Boissieu, M. Boudard, H. Vincent, M. Durand, J.M. Dubois, and C. Dong, J. Non-Cryst. Solids **150**, 322 (1992).
[24] A. Katz and D. Gratias, J. Non-Cryst. Solids **153& 154**, 187 (1993).
[25] K. Hiraga, in *Aperiodic '94*, edited by G. Chapuis and W. Paciorek (World Scientific, Singapore, 1995), pp. 341–350.
[26] K. Saitoh, K. Tsuda, M. Tanaka, A.P. Tsai, A. Inoue, and T. Masumoto, Philos. Mag. A **73**, 387 (1996).
[27] K. Saitoh, K. Tsuda, M. Tanaka, K. Kaneko, and A.P. Tsai, Jpn. J. Appl. Phys., Part 2 **36**, L1400 (1997).
[28] A. Yamamoto, A. Sato, K. Kato, A. P. Tsai, and T. Masumoto, in *Quasicrystals and Imperfectly Ordered Crystals*, edited by K. H. Kuo and S. Takeuchi (Trans Tech, Aedermannsdorf, 1994), Vol. 150-151, pp. 211–222.
[29] A. Yamamoto and K. Hiraga, Mater. Sci. Eng., A **294-296**, 228 (2000).
[30] A. Yamamoto, Y. Matsuo, T. Yamanoi, A. P. Tsai, K. Hiraga, and T. Masumoto, in *Aperiodic '94*, edited by G. Chapuis and W. Paciorek (World Scientific, Singapore, 1995), pp. 393–398.
[31] C.l. Henley and V. Elser, Philos. Mag. B **53**, L59 (1986).
[32] K. Sugiyama, N. Kaji, K. Hiraga, and T. Ishimasa, Z. Kristallogr. **213**, 90 (1998).
[33] K. Sugiyama, W. Sun, and K. Hiraga, J. Alloys Compd. **342**, 139 (2002).
[34] V. Elser, Phys. Rev. B **32**, 4892 (1985).
[35] T. Janssen, Philos. Mag. Lett. **66**, 125 (1992).
[36] D. Gratias, J.W. Cahn, and B. Mozer, Phys. Rev. B **38**, 1638 (1988).
[37] H. Takakura, M. Shiono, T.J. Sato, A. Yamamoto, and A.P. Tsai, Phys. Rev. Lett. **86**, 236 (2001).
[38] A. Katz and M. Duneau, J. Phys. (Paris) **47**, 181 (1986).
[39] T. Ogawa, J. Phys. Soc. Jpn. **54**, 3205 (1985).
[40] A. Yamamoto, Phys. Rev. B **45**, 5217 (1992).
[41] C.L. Henley, Phys. Rev. B **34**, 797 (1986).

[42] K. Hiraga, in *Quasicrystals*, edited by J. M. Dubois, P. A. Thiel, A. P. Tsai, and K. Urban (Materials Research Society, Warrendale, Pennsylvania, 1999), pp. 107–116.
[43] Y. Ishii, Phys. Rev. B **39**, 11 862 (1989).
[44] K. Niizeki, J. Phys. A **24**, 3641 (1991).
[45] C.L. Henley, Phys. Rev. B **43**, 993 (1991).
[46] M. Mihalkovic and P. Mrafko, Philos. Mag. Lett. **69**, 85 (1994).
[47] M. Mihalkovic and P. Mrafko, Phys. Rev. B **49**, 100 (1994).
[48] D. Gratias, F. Puyraimond, M. Quiquandon, and A. Katz, Phys. Rev. B **63**, 024202 (2001).
[49] C.P. Gomez and S. Lidin, Angew. Chem., Int. Ed. **40**, 4037 (2001).